

Syntheses and Phosphorescent Properties of Blue Emissive Iridium Complexes with Tridentate Pyrazolyl Ligands

Lifen Yang,[†] Fumio Okuda,[§] Katsuaki Kobayashi,[†] Koichi Nozaki,^{**‡} Yoshiaki Tanabe,[†] Youichi Ishii,[†] and Masa-aki Haga^{*}

Department of Applied Chemistry, Faculty of Science and Engineering, Chuo University, 1-13-27, Kasuga, Bunkyo-ku, Tokyo 112-8551, Japan, Department of Chemistry, Graduate School of Science and Engineering, University of Toyama, 3190, Gofuku, Toyama-shi, Toyama 930-8555, Japan, and Central Research Laboratories, Idemitsu Kosan Co., Ltd., 1280 Kami-Izumi, Sodegaura, Chiba 299-0293, Japan

Received January 30, 2008

Novel neutral mixed-ligand Ir(N[^]C[^]N)(N[^]C)X complexes (N[^]C[^]N = 1,3-bis(3-methylpyrazolyl)benzene (bpbz), 1,5-dimethyl-2,4-bis(3-methylpyrazolyl)benzene (dmbpbz), and 1,5-difluoro-2,4-bis(3-methylpyrazolyl)benzene (dfbpbz); N[^]C = 2-phenyl pyridine (ppy); and X = Cl or CN) have been synthesized and characterized. An X-ray single-crystal structure of the complex Ir(dmbpbz)(ppy)Cl shows that the nitrogen atom in the ppy ligand occupied the trans position to the carbon atom in the tridentate N[^]C[^]N ligand of dmbpbz with the Ir–C bond length of 1.94(1) Å, whereas the coordinating carbon atom occupied the trans position of chlorine. Electrochemical data show that the complexes exhibit an oxidation Ir(III/IV) process in the potential range of +0.5~0.9 V and two irreversible reductions at approximately –2.6 and –3.0 V against Fc⁰/Fc⁺, respectively. All of the Ir(III) complexes do not emit phosphorescence at room temperature, although strong phosphorescence is exhibited at 77 K with the 0–0 transition centered at around 450 nm and lifetimes of 3–14 μs. DFT calculations indicate that the HOMOs are mainly localized on iridium 5dπ and chlorine pπ*, whereas the LUMOs are mainly from the ppy ligand π* orbitals. The phosphorescence originates from a ³LC state mixed with the ³MLCT and ³XLCT ones. Temperature-dependent lifetime measurements of Ir(dfbpbz)(ppy)Cl reveal the existence of a thermal deactivation process with a low activation energy (1720 cm⁻¹) and very high frequency factor (2.3 × 10¹³ s⁻¹). An unrestricted density functional theory indicates that the dd state, in which both the Ir–N (pyrazolyl) bond lengths increase considerably, exists almost at the same energy as that for the phosphorescent state. A thorough analysis based on the potential energy surfaces for the T₁ and S₀ states allows us to determine the reaction pathway responsible for this thermal deactivation. The calculated activation energies of 1600~1800 cm⁻¹ are in excellent agreement with the observed values.

Introduction

Iridium complexes with cyclometalating ligands have attracted considerable attention for their potential application in electrophosphorescent organic light-emitting diodes (OLEDs).^{1–4} Because the optical properties and related applications of cyclometalated iridium complexes are strongly

dependent on the characteristics of their ground and lowest excited states, it has been well demonstrated that the structural changes in the skeletal structure and the substituent groups of the cyclometalating ligand afford significant color tuning of electrophosphorescence.⁵ Recently, researchers have focused upon the preparation and characterization of

* To whom correspondence should be addressed: E-mail: mhaga@chem.chuo-u.ac.jp (M.H.), nozaki@sci.u-toyama.ac.jp (K.N.).

[†] Chuo University.

[§] Idemitsu Kosan Co.

[‡] University of Toyama.

(1) (a) Ren, X.; Li, J.; Holmes, R. J.; Djurovich, P. I.; Forrest, S. R.; Thompson, M. E. *Chem. Mater.* **2004**, *16*, 4743. (b) Sajoto, T.; Djurovich, P. I.; Tamayo, A.; Yousufuddin, M.; Bau, R.; Thompson, M. E.; Holmes, R. J.; Forrest, S. R. *Inorg. Chem.* **2005**, *44*, 7992.

(2) Su, Y.-J.; Huang, H.-L.; Li, C.-L.; Chien, C.-H.; Tao, Y.-T.; Chou, P.-T.; Datta, S.; Liu, R.-S. *Adv. Mater.* **2003**, *15*, 884.

(3) Rayabarapu, D. K.; Paulose, B. M. J. S.; Duan, J. P.; Cheng, C. H. *Adv. Mater.* **2005**, *17*, 349.

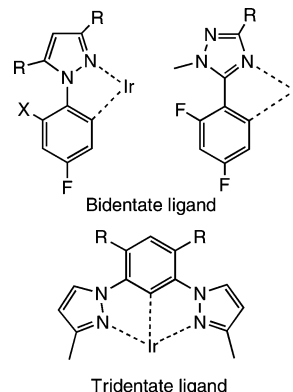
(4) (a) Evans, R. C.; Douglas, P.; Winscom, C. J. *Coord. Chem. Rev.* **2006**, *250*, 2093. (b) Lowry, M. S.; Bernhard, S. *Chem.—Eur. J.* **2006**, *12*, 7970. (c) Chou, P.-T.; Chi, Y. *Chem.—Eur. J.* **2007**, *13*, 380.

(5) You, Y.; Park, S. Y. *J. Am. Chem. Soc.* **2005**, *127*, 12438.

blue-emitting phosphorescent complexes.^{6–10} To synthesize these complexes, the following guideline for molecular design is considered: (1) introduction of the ligand with higher π^* energies or larger $\pi\pi^*$ energy gap and (2) selection of strong donor atoms such as carbon anions or carbene carbon. Several blue emissive iridium complexes have been synthesized using the bidentate triazolyl pyridine derivatives or introducing electron-rich groups such as ancillary ligands^{6,7} as well as through various electron-withdrawing groups such as fluoro groups at the bidentate phenylpyridine ligand.^{8–10} Compared to the tris-bidentate iridium complexes, iridium complexes with tridentate ligands are still limited, whereas many articles on tridentate Pt(II)^{9,11–20} and Ru(II) complexes^{21–23} have been reported.

Recently, we have reported the synthesis of highly emissive iridium complexes [Ir(L)(ppy)X] (L = bis(*N*-methylbenzimidazolyl)-benzene (Mebib) or -pyridine (Me-bip), ppy = 2-phenylpyridine) in which the substitution from L = Mebip (N \wedge N \wedge N coordination mode) to Mebib (N \wedge C \wedge N mode) induced a blue shift in the emission maxima.^{24,38} All of the complexes, [Ir(Mebib)(ppy)X], yielded high luminescent quantum yield $\Phi = 0.77\sim 0.86$. Further, a change in the coordination group in the tridentate ligand N \wedge C \wedge N from benzimidazole to pyridine results in a shorter-wavelength

Chart 1. Bidentate and Tridentate Ligand Systems Containing Pyrazole or Triazole Ring(s)



shift in the emission maximum.²⁵ In the case of the emissive tris-bidentate type of iridium complexes, phenylpyrazole or phenyltriazole derivatives (Chart 1) have been used for the synthesis of blue iridium phosphors.^{6,7} Because the alteration of the *N*-heterocyclic ring system in the tridentate N \wedge C \wedge N ligand can tune the emission maximum onto a shorter wavelength, replacing the benzimidazole or pyridine moieties with pyrazole groups in the N \wedge C \wedge N ligand may anticipate a further blue shift in the emission wavelength because of higher π^* orbital energies of pyrazoles than those of pyridines. In this article, we report the synthesis and the photophysical and electrochemical properties of blue emissive Ir(III) complexes containing both tridentate bis(pyrazolyl)benzene (N \wedge C \wedge N) and bidentate phenylpyridine (N \wedge C) ligands (Chart 2). To demonstrate the deactivation process at the excited state, temperature-dependent measurements of the emission lifetime and theoretical DFT calculations for the potential energy curves have been studied.

Experimental Section

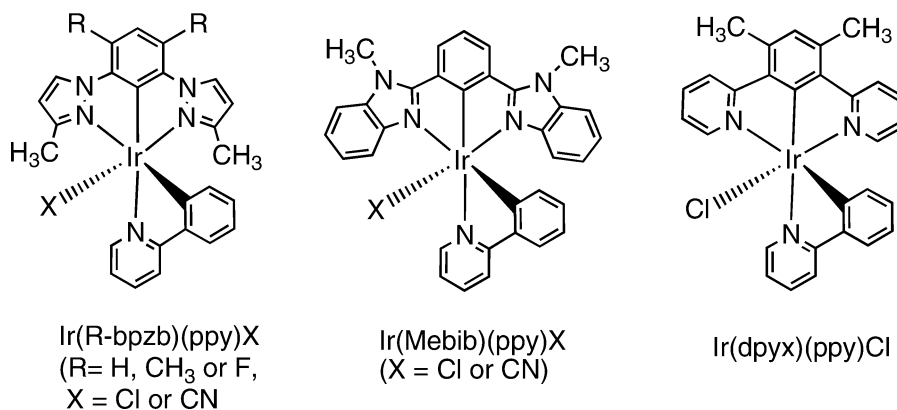
Materials. IrCl₃·*n*H₂O (Heraeus), 1,3-dibromobenzene (TCI), 3-methylpyrazole (TCI), trans-1,2-cyclohexanediamine (TCI), and copper (I) iodide (Kanto) were used as received. 2,4-Difluoro-1,5-dibromobenzene²⁶ and 1,5-dibromo-2,4-dimethyl-benzene²⁷ were synthesized according to the methods described in the literature. For the photophysical measurements, spectroscopic-grade 1,2-dichloromethane and toluene were purchased from Nacalai Tesque Inc., Kyoto, Japan. For the electrochemical measurements, *N,N*-dimethylformamide (DMF) for nonaqueous titrimetry (Nacalai) was used as supplied, and tetra-*n*-butylammonium tetrafluoroborate (Nacalai) was purified by recrystallization from EtOH and dried before use.

Physical Measurements. The ¹H NMR, ESI-MS, MALDI-TOF-MS, and UV–vis spectra were recorded with a JNM-ECA 500 (JEOL) spectrometer, a Micromass electrospray LCT, Shimadzu MALDI-TOF AXIMA-CFR mass spectrometer, and Jasco V530 UV–vis spectrophotometer, respectively. The electrochemical measurements were carried out in a standard one-compartment cell under N₂ gas flow equipped with a BAS glass-carbon ($\varphi = 3$ mm) working electrode, Pt-wire counter electrode, and Ag/Ag⁺ reference

- (7) (a) Yang, C.-H.; Li, S.-W.; Chi, Y.; Cheng, Y.-M.; Yeh, Y.-S.; Chou, P.-T.; Lee, G.-H.; Wang, C.-H.; Shu, C.-F. *Inorg. Chem.* **2005**, *44*, 7770. (b) Takizawa, S.; Echizen, H.; Nishida, J.; Tsuzuki, T.; Tokito, S.; Yamashita, Y. *Chem. Lett.* **2006**, *35*, 748. (c) Lo, S.-C.; Shipley, C. P.; Bera, R. N.; Harding, R. E.; Cowley, A. R.; Burn, P. L.; Samuel, I. D. W. *Chem. Mater.* **2006**, *18*, 5119.
- (8) (a) Tamayo, A. B.; Alleyne, B. D.; Djurovich, P. I.; Lamansky, S.; Tsyba, I.; Ho, N. N.; Bau, R.; Thompson, M. E. *J. Am. Chem. Soc.* **2003**, *125*, 7377. (b) Lo, S.-C.; Richards, G. J.; Markham, P. J.; Namdas, E. B.; Sharma, S.; Burn, P. L.; Samuel, I. D. W. *Adv. Funct. Mater.* **2005**, *15*, 1451. (c) Ragni, R.; Plummer, E. A.; Brunner, K.; Hofstraat, J. W.; Babudri, F.; Farinola, G. M.; Naso, F.; De Cola, L. *J. Mater. Chem.* **2006**, *16*, 1161.
- (9) Coppo, P.; Plummer, E. A.; De Cola, L. *Chem. Commun.* **2004**, 1774.
- (10) (a) Dedeian, K.; Shi, J.; Shepherd, N.; Forsythe, E.; Morton, D. C. *Inorg. Chem.* **2005**, *44*, 4445. (b) Dedeian, K.; Shi, J.; Forsythe, E.; Morton, D. C.; Zavalij, P. Y. *Inorg. Chem.* **2007**, *46*, 1603.
- (11) Arena, G.; Calogero, G.; Campagna, S.; Scolaro, L. M.; Ricevuto, V.; Romeo, R. *Inorg. Chem.* **1998**, *37*, 2763.
- (12) Michalec, J. F.; Bejune, S. A.; Cuttill, D. G.; Summerton, G. C.; Gertenbach, J. A.; Field, J. S.; Haines, R. J.; McMillin, D. R. *Inorg. Chem.* **2001**, *40*, 2193.
- (13) Hofmann, A.; Dahlenburg, L.; van Eldik, R. *Inorg. Chem.* **2003**, *42*, 6528.
- (14) Wong, K. M.-C.; Tang, W.-S.; Lu, X.-X.; Zhu, N.; Yam, V. W.-W. *Inorg. Chem.* **2005**, *44*, 1492.
- (15) Grove, L. J.; Rennekamp, J. M.; Jude, H.; Connick, W. B. *J. Am. Chem. Soc.* **2004**, *126*, 1594.
- (16) Yam, V. W. W.; Wong, K. M.-C.; Zhu, N. *Angew. Chem. Int. Ed.* **2003**, *42*, 1400.
- (17) Yang, Q.-Z.; Wu, L.-Z.; Wu, Z.-X.; Zhang, L.-P.; Tung, C.-H. *Inorg. Chem.* **2002**, *41*, 5653.
- (18) Michalec, J. F.; Bejune, S. A.; McMillin, D. R. *Inorg. Chem.* **2000**, *39*, 2708.
- (19) Yam, V. W.; Wog, K. M.-C.; Zhu, N.; Tang, R. P.-L.; Wong, K. M.-C.; Cheung, K.-K. *Organometallics* **2001**, *20*, 4476.
- (20) Lu, W.; Mi, B.-X.; Chan, M. C. W.; Hui, Z.; Zhu, N.; Lee, S.-T.; Che, C.-M. *Chem. Commun.* **2002**, 206.
- (21) Chanda, N.; Paul, D.; Kar, S.; Mobin, S. M.; Datta, A.; Puranik, V. G.; Rao, K. K.; Lahiri, G. K. *Inorg. Chem.* **2005**, *44*, 3499.
- (22) Bonnet, S.; Collin, J.-P.; Sauvage, J.-P.; Schofield, E. *Inorg. Chem.* **2004**, *43*, 8346.
- (23) Son, S. U.; Park, K. H.; Lee, Y.-S.; Kim, B. Y.; Choi, C. H.; Lah, M. S.; Jang, Y. H.; Jang, D.-J.; Chung, Y. K. *Inorg. Chem.* **2004**, *43*, 6896.
- (24) Yutaka, T.; Obara, S.; Ogawa, S.; Nozaki, K.; Ikeda, N.; Ohno, T.; Ishii, Y.; Sakai, K.; Haga, M. *Inorg. Chem.* **2005**, *44*, 4737.

(25) Wilkinson, A. J.; Puschmann, H.; Howard, J. A. K.; Foster, C. E.; Williams, J. A. G. *Inorg. Chem.* **2006**, *45*, 8685.

(26) Wang, Z.-X.; Duan, W. D.; Wiebe, L. I.; Balzarini, J.; Clercq, E. D.; Knaus, E. E. *Nucleosides, Nucleotides & Nucleic Acids* **2001**, *20*, 11.

Chart 2. Chemical Structures of $[\text{Ir}(\text{N}\wedge\text{C}\wedge\text{N})(\text{N}\wedge\text{C})\text{X}]$ 

electrode along with an ALS/CH model 660A electrochemical analyzer. The reference electrode was Ag/AgNO_3 (0.01 M in 0.1 M $\text{TBABF}_4 \cdot \text{CH}_3\text{CN}$), which was abbreviated as Ag/Ag^+ . The ferrocene/ferrocenium (Fc^0/Fc^+) redox potential was used as the internal reference standard, and all the potentials were reported against Fc^0/Fc^+ . The emission spectra were recorded using a grating monochromator (Triax 1900, Jobin Yvon) with a CCD image sensor (S7031, Hamamatsu). The spectral sensitivity of the spectrofluorometer was corrected using a bromine lamp (IPD 100V 500WCS, Ushio). A sample solution in a 1 mm quartz cell was deoxygenated and excited using an LD-excited solid-state Q-switched Nd:YVO₄ laser (355 nm, 400 ps, 13 kHz, and 6 mW; JDS Uniphase).

For performing the emission lifetime measurements, a deoxygenated sample solution was photoexcited using the Nd:YVO₄ laser. The emission from the sample was monochromated using a grating monochromator (H-20, Jobin Yvon) and converted into current signals by a photomultiplier tube (R9110, Hamamatsu). The transient signal for 2560–10 240 shots were accumulated on a digitizing oscilloscope (HP 54520 Hewlett-Packard) to obtain the decay profile of the emission intensity, which was fitted to two or three exponential functions by the convolution of the instrumental response function of the measuring system. The time resolution of the system is 2 ns. The measurements of the emission lifetimes and spectra at 77 K were performed using a cylindrical quartz cell (inner diameter: 1 mm) and a liquid-nitrogen dewar. Emission lifetimes in the range of 90–300 K were measured for a deoxygenated sample solution in a 1 cm cell set in a cryostat (Oxford DN1704), and the temperature of the sample was controlled within 0.2 °C using a controller (Oxford ITC4).

The DFT calculations were performed by the *Gaussian 03* suite²⁸ using a hybrid density functional PBE1PBE. Two types of basis sets were employed. For the geometry optimizations, Gaussian-type orbital (GTO) basis sets of Dunning–Hay’s split-valence double- ζ (D95) were used for carbon, hydrogen, nitrogen, and fluorine atoms and Hay–Wadt double- ζ functions with Los Alamos relativistic effective core potential were used for the iridium and chlorine atoms (BSI). The energy calculations were performed with large basis sets (BSII), in which the d-type polarization functions were added to the D95 basis sets (D95*) for light atoms and triple- ζ functions with relativistic effective pseudopotential reported by the Stuttgart group (Stuttgart RSC 1997)²⁹ were used for the iridium and chlorine atoms.

Crystal-Structure Determination. Single crystals of $\text{Ir}(\text{dfbpzb})(\text{ppy})\text{Cl}$ and $\text{Ir}(\text{dmbpzb})(\text{ppy})\text{Cl} \cdot \text{CH}_2\text{Cl}_2$ suitable for X-ray crystallography were obtained by the slow diffusion of methanol or hexane into the corresponding dichloromethane solution. The diffraction

data for both the crystals were collected using a Rigaku Mercury CCD area detector with graphite monochromated Mo $\text{K}\alpha$ radiation ($\lambda = 0.7107 \text{ \AA}$) at $-150 \pm 1 \text{ }^\circ\text{C}$, except that the maximum 2θ value for the former crystal is 63.3° and for the latter one is 63.5° .

The structure solution and refinements were carried out using the *Crystal Structure* crystallographic software package.^{30,31} The structures were solved using direct methods and expanded using Fourier techniques. Some non-hydrogen atoms were refined anisotropically, whereas the remaining atoms were refined isotropically. The hydrogen atoms were refined using the riding model. The structure refinement of the crystal structure for $\text{Ir}(\text{dfbpzb})(\text{ppy})\text{Cl}$ was unsuccessful even though the approximate geometry of $\text{Ir}(\text{dfbpzb})(\text{ppy})\text{Cl}$ was obtained. The crystal data and structure refinement for $\text{Ir}(\text{dmbpzb})(\text{ppy})\text{Cl} \cdot \text{CH}_2\text{Cl}_2$ are summarized in Table 1.

Syntheses. The tridentate $\text{N}\wedge\text{C}\wedge\text{N}$ ligands were synthesized in light of the reported method by the coupling of 1,3-bromobenzene or its derivatives with 3-methylpyrazole using CuI and diimine as the catalyst.^{32–34}

1,3-Bis(3-methylpyrazolyl)benzene (bpzb). 1,3-Dibromobenzene (2.56 g, 10 mmol), 3-methylpyrazole (2.60 g, 32 mmol), CuI (0.29 g, 1.5 mmol), and *trans*-1,2-cyclohexanediamine (0.85 g, 6 mmol) were added successively to dry K_2CO_3 (6.0 g, 43 mmol) in

(27) Negoro, T.; Takaoka, S.; Hayashi, S.; Urata, H. *Bull. Fac. Edu. Wakayama Univ. Natur. Sci.* **2002**, *52*, 27.

(28) Frisch, M. J.; Trucks, F. W.; Schlegel, H. B.; Scuseria, G. E.; Robb, M. A.; Cheeseman, J. R.; Montgomery, J., J. A.; Vreven, T.; Kudin, K. N.; Burant, J. C.; Millam, J. M.; Iyengar, S. S.; Tomasi, J.; Barone, V.; Mennucci, B.; Cossi, M.; Scalmani, G.; Rega, N.; Petersson, G. A.; Nakatsuji, H.; Hada, M.; Ehara, M.; Toyota, K.; Fukuda, R.; Hasegawa, J.; Ishida, M.; Nakajima, T.; Honda, Y.; Kitao, O.; Nakai, H.; Klene, M.; Li, X.; Knox, J. E.; Hratchian, H. P.; Cross, J. B.; Bakken, V.; Adamo, C.; Jaramillo, J.; Gomperts, R.; Stratmann, R. E.; Yazyev, O.; Austin, A. J.; Cammi, R.; Pomelli, C.; Ochterski, J. W.; Ayala, P. Y.; Morokuma, K.; Voth, G. A.; Salvador, P.; Dannenberg, J. J.; Zakrzewski, V. G.; Dapprich, S.; Daniels, A. D.; Strain, M. C.; Farkas, O.; Malick, D. K.; Rabuck, A. D.; Raghavachari, K.; Foresman, J. B.; Ortiz, J. V.; Cui, Q.; Baboul, A. G.; Clifford, S.; Cioslowski, J.; Stefanov, B. B.; Liu, G.; Liashenko, A.; Piskorz, P.; Komaromi, I.; Martin, R. L.; Fox, D. J.; Keith, T.; Al-Laham, M. A.; Peng, C. Y.; Nanayakkara, A.; Challacombe, M.; Gill, P. M. W.; Johnson, B.; Chen, W.; Wong, M. W.; Gonzalez, C.; Pople, J. A. *Gaussian 03, revision C.01* 2004, Gaussian, Inc., Wallingford, CT.

(29) The EMSL Gaussian Basis Set Library at <http://www.emsl.pnl.gov/forms/basisform.html>.

(30) *Crystal Structure 3.8: Crystal Structure Analysis Package*; R. a. R. M.: The Woodlands, TX, USA, 2000–2004.

(31) Carruthers, J.; Rollett, J. S.; Betteridge, J.; Kinna, D.; Pearce, J.; Larsen, A.; GabeCRYSTALS; Issue 10 1, p 999.

(32) Klapars, A.; Antilla, J. C.; Huang, X.; Buchwald, S. L. *J. Am. Chem. Soc.* **2001**, *123*, 7727.

(33) Antilla, J. C.; Baskin, J. M.; Barder, T. E.; Buchwald, S. L. *J. Org. Chem.* **2004**, *69*, 5578.

(34) Cristau, H.-J.; Cellier, P. P.; Spindler, J.-F.; Taillefer, M. *Eur. J. Org. Chem.* **2004**, 695.

Table 1. Crystallographic Data for Complex Ir(dmbpzb)(ppy)Cl·CH₂Cl₂

	Ir(dmbpzb)(ppy)Cl·CH ₂ Cl ₂
chemical formula	C ₂₈ H ₂₇ N ₅ Cl ₃ Ir
fw	732.13
cryst color, habit	yellow, prism
cryst dimensions	0.25 × 0.15 × 0.10 mm ³
cryst syst	triclinic
space group	P $\bar{1}$
<i>a</i> (Å)	8.182(11)
<i>b</i> (Å)	12.73(2)
<i>c</i> (Å)	14.200(10)
α (deg)	69.38(13)
β (deg)	79.73(9)
γ (deg)	86.91(13)
<i>V</i> (Å ³)	1362.4(30)
<i>Z</i>	2
<i>D</i> _{calcd} (g/cm ³)	1.785
<i>F</i> ₀₀₀	716.00
R1 [<i>I</i> < 3.0 σ (<i>I</i>)]	0.054
GOF	1.000

a Schlenk tube. The mixture was heated at 110 °C for 24 h under nitrogen. After cooling to the ambient temperature, ethyl acetate was added to the reaction mixture. The resulting solution was filtered through a plug of silica gel, and the adsorbate was eluted with 100 mL of ethyl acetate. The filtrate was concentrated, and the resulting residue was purified by column chromatography with a hexane–ethyl acetate mixture (5:1 v/v). The target compound was obtained as colorless oil (1.14 g, 47.2%). ¹HNMR (500 MHz, CDCl₃) δ : 7.99 (t, 1H, *J* = 2.5 Hz), 7.89 (d, 2H, *J* = 2 Hz), 7.53 (m, 2H), 7.45 (m, 1H), 6.26 (d, 2H, *J* = 2.5 Hz), 2.38 (s, 6H). ESI-MS *m/z* 239.0138 (239.1297 required for [C₁₄H₁₅N₄]⁺).

1,5-Difluoro-2,4-bis(3-methylpyrazolyl)benzene (dfbpzb). The synthesis procedure is similar to that described above, except that 2,4-difluoro-1,5-dibromobenzene was used instead of 1,3-dibromobenzene. Yield: 15.4%. ¹HNMR (500 MHz, CDCl₃) δ : 8.30 (t, 1H, *J* = 8 Hz), 7.78 (s, 1H), 7.06 (t, 1H, *J* = 11 Hz), 6.20 (d, 2H, *J* = 3 Hz), 2.30 (s, 6H). ESI-MS *m/z* 274.9401 (275.1108 required for [C₁₄H₁₃F₂N₄]⁺). Anal. Calcd for C₁₄H₁₂F₂N₄: C, 61.31; H, 4.41; N, 20.43. Found: C, 60.90; H, 4.36; N, 20.13.

1,5-Dimethyl-2,4-bis(3-methylpyrazolyl)benzene (dmbpzb). This compound was obtained in a manner similar to dfbpzb, except that 1,5-dibromo-2,4-dimethylbenzene was used. Yield: 19%. ¹HNMR (500 MHz, CDCl₃) δ : 7.40 (d, 2H, *J* = 2 Hz), 7.24 (s, 1H), 7.13 (s, 1H), 6.11 (d, 2H, *J* = 2 Hz), 2.27 (s, 6H), 2.17 (s, 6H). ESI-MS *m/z* 266.9518 (267.1610 required for [C₁₆H₁₉N₄]⁺).

[Ir(bpzb)Cl₂]₂, IrCl₃·*n*H₂O (1.40 g, 3.90 mmol) and bpzb (1.14 g, 4.76 mmol) were refluxed in methanol for 15 h. After cooling to room temperature, the green precipitate was collected and then washed by methanol followed by ether. Yield (1.08 g, 27.6%). This complex is insoluble in common organic solvents; therefore, this compound was used without further purification.

[Ir(L)Cl₂]₂ (L = dmbpzb or dfbpzb). This compound was obtained similar to the procedure described above, except that dmbpzb or dfbpzb was used as the ligand. Yield: 39% (L = dmbpzb) and 34% (L = dfbpzb). This complex was used as the starting material for the next step without further purification.

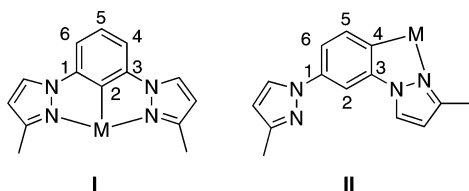
Ir(dmbpzb)(ppy)Cl. The mixture of Ir₂(dmbpzb)₂Cl₄ (0.12 g, 0.11 mmol) and ppy (0.04 g, 0.27 mmol) in glycerol (30 mL) was irradiated with microwave radiation (650 W) for 9 min. After being cooled to room temperature, the addition of saturated NaCl aqueous solution afforded a yellow precipitate, which was collected and washed with hexane and ether. The purification was performed by recrystallization from CH₂Cl₂–hexane twice, which yielded yellow

crystalline materials. Yield: 0.12 g (84%). ¹HNMR (CDCl₃, 500 MHz), δ : 10.30 (d, 1H), 7.95 (t, 3H, *J* = 7.5 Hz), 7.82 (t, 1H, *J* = 7.5 Hz), 7.54 (d, 1H, *J* = 8 Hz), 7.38 (t, 1H, *J* = 8 Hz), 6.69 (m, 2H), 6.56 (t, 1H), 6.02 (d, 1H, *J* = 2.6 Hz), 5.95 (d, 2H, *J* = 2.4 Hz), 2.61 (s, 6H), 1.55 (s, 6H). Anal. Calcd for C₂₇H₂₅ClIrN₅·0.5CH₂Cl₂·0.5C₆H₁₂: C, 50.06; H, 4.00; N, 9.58. Found: C, 49.98; H, 3.81; N, 9.92. MALDI-TOF MS *m/z* 611.46 ([M–Cl]⁺, M = [C₂₇H₂₅IrN₅Cl]).

Ir(dfbpzb)(ppy)Cl. The mixture of [Ir(dfbpzb)₂Cl₂]₂ (0.23 g, 0.21 mmol) and ppy (0.12 g, 0.75 mol) in glycerol (30 mL) was heated by the microwave irradiation (650 W) for 9 min. After cooling to room temperature, a saturated aqueous solution of NaCl (50 mL) was added to yield a greenish-yellow precipitate. The precipitate was collected by filtration, and washed with hexane and ether. Recrystallization from CH₂Cl₂–hexane afforded a greenish-yellow powder. Yield: 0.22 g, 80%. ¹HNMR (CDCl₃, 500 MHz), δ : 10.27 (d, 1H, *J* = 5.5 Hz), 7.97 (d, 1H, *J* = 8 Hz), 7.93 (d, 2H, *J* = 2.5 Hz), 7.86 (ddd, 1H, *J*₁ = 7.6 Hz, *J*₂ = 4.7 Hz, *J*₃ = 1.1 Hz), 7.55 (d, 1H, *J* = 17 Hz), 7.42 (dd, 1H, *J*₁ = 7.8 Hz, *J*₂ = 1.4 Hz), 6.81 (t, 1H, *J* = 10.5 Hz), 6.74 (t, 1H, *J* = 7.5 Hz), 6.61 (t, 1H, *J* = 7.5 Hz), 6.02 (d, 1H, *J* = 7.5 Hz), 5.97 (d, 2H, *J* = 2.5 Hz), 1.55 (s, 6H). Anal. Calcd for C₂₅H₁₉ClF₂IrN₅·H₂O: C, 44.61; H, 3.14; N, 10.40. Found: C, 44.65; H, 2.90; N, 10.18. MALDI-TOF MS *m/z* 619.80 ([M–Cl]⁺, M = [C₂₅H₁₉IrN₅F₂Cl]).

Ir(bpzb)(ppy)CN. A mixture of [Ir(bpzb)Cl₂]₂ (0.26 g, 0.25 mol) and ppy (0.12 g, 0.75 mol) in glycerol (30 mL) was heated by microwave irradiation (650 W, multimode) for 4.5 min. After cooling to room temperature, water (50 mL) and saturated NaCl solution (20 mL) were added to yield a greenish-yellow precipitate, which was collected by filtration. ¹HNMR shows that this was a mixture of several complexes such as Ir(bpzb)(ppy)Cl and Ir₂(ppy)₄Cl₂ dimers. The use of column chromatography to purify the target compound has proven unsuccessful; therefore, the mixture was used in the following metathesis reaction. The mixture mentioned above (0.10 g, 0.15 mmol) and KCN (0.40 g) in ethylene glycol was irradiated with microwave radiation (650 W) for 3 min. After cooling to room temperature, a saturated aqueous solution of NaCl (50 mL) was added. The mixture was extracted with dichloromethane to yield a crude product. The product obtained was washed with water, ether, and then recrystallized from dichloromethane–hexane several times. Yield: 75 mg (24%). ¹HNMR (500 MHz, CDCl₃) δ : 10.32 (d, 1H, *J* = 5.5 Hz), 8.04 (d, 1H, *J* = 7.5 Hz), 7.94 (ddd, 1H, *J*₁ = 7.5 Hz, *J*₂ = 4.6 Hz, *J*₃ = 1.3 Hz), 7.87 (d, 2H, *J* = 2.5 Hz), 7.66 (d, 1H, *J* = 8 Hz), 7.41 (ddd, 1H, *J*₁ = 7.5 Hz, *J*₂ = 5.0 Hz, *J*₃ = 1.3 Hz), 7.17 (d, 2H, *J* = 8 Hz), 6.85 (ddd, 1H, *J*₁ = 7.5 Hz, *J*₂ = 5 Hz, *J*₃ = 1 Hz), 6.70 (ddd, 1H, *J*₁ = 7.5 Hz, *J*₂ = 4.6 Hz, *J*₃ = 1.3 Hz), 6.05 (d, 2H, *J* = 2.5 Hz), 6.02 (d, 1H, *J* = 7.5 Hz), 2.17 (s, 6H). FT-IR (KBr pellet): ν (C≡N): 2100.59 cm⁻¹. Anal. Calcd for C₂₆H₂₁IrN₆·H₂O: C, 49.75; H, 3.69; N, 13.39. Found: C, 50.18; H, 3.54; N, 13.68. MALDI-TOF-MS *m/z* 583.57 ([M–CN]⁺, M = [C₂₅H₂₁IrN₅CN]).

Ir(dfbpzb)(ppy)CN. A mixture of Ir(dfbpzb)(ppy)Cl (0.17 g, 0.26 mmol) and KCN (0.04 g, 0.58 mmol) in ethylene glycol (20 mL) was heated by microwave irradiation (650 W) for 3 min. After cooling to room temperature, a pale greenish-yellow crude product was precipitated upon the addition of a saturated aqueous solution of NaCl (50 mL). The obtained precipitate was filtered and washed by hexane followed by ether. The crude product was purified by recrystallization from CH₂Cl₂–hexane to afford a faint-yellow powder. Yield: 43 mg (26%). ¹HNMR (500 MHz, CDCl₃) δ (ppm): 10.29 (d, 1H, *J* = 5.5 Hz), 7.97 (m, 3H), 7.96 (ddd, 1H, *J*₁ = 7.5 Hz, *J*₂ = 5 Hz, *J*₃ = 1 Hz), 7.68 (d, 1H, *J* = 8 Hz), 7.42 (ddd, 1H, *J*₁ = 7.5 Hz, *J*₂ = 4.7 Hz, *J*₃ = 1.2 Hz), 6.91 (m, 2H), 6.78 (ddd,

Scheme 1. Two Coordination Modes of bpzb Ligand.

1H, $J_1 = 7.5$ Hz, $J_2 = 5.0$ Hz, $J_3 = 1.2$ Hz), 6.10 (dd, 1H, $J_1 = 7.5$ Hz, $J_2 = 2.2$ Hz), 6.06 (d, 2H, $J = 3$ Hz), 1.61 (s, 6H). FT-IR (KBr pellet): ν (C \equiv N): 2115.41 cm^{-1} . Anal. Calcd for $\text{C}_{26}\text{H}_{19}\text{F}_2\text{IrN}_6 \cdot \text{H}_2\text{O}$: C, 47.05; H, 3.19; N, 12.66. Found: C, 47.04; H, 2.87; N, 12.33. MALDI-MS m/z 619.70 ($[\text{M}-\text{CN}]^+$, $\text{M} = [\text{C}_{25}\text{H}_{19}\text{IrF}_2\text{N}_5\text{CN}]$).

Ir(dmbpzb)(ppy)CN. The synthesis procedure was the same as that used for Ir(dfbpzb)(ppy)CN, except for substituting Ir(dfbpzb)(ppy)Cl for Ir(dmbpzb)(ppy)Cl. A faint-yellow powder was obtained by recrystallization from CH_2Cl_2 –hexane. Yield: 27%. ^1H NMR (500 MHz, CDCl_3), δ : 10.30 (d, 1H, $J = 6$ Hz), 8.03 (d, 2H, $J = 3.5$ Hz), 7.92 (t, 1H, $J = 8.5$ Hz), 7.66 (d, 1H, $J = 8$ Hz), 7.39 (t, 1H, $J = 7$ Hz), 6.85 (t, 1H, $J = 8$ Hz), 6.81 (s, 1H), 6.72 (t, 1H, $J = 7.5$ Hz), 6.10 (d, 1H, $J = 7.5$ Hz), 6.02 (d, 2H, $J = 2.5$ Hz), 5.30 (s, 1H), 2.67 (s, 6H), 1.61 (s, 6H). FT-IR (KBr pellet): ν (C \equiv N): 2104.43 cm^{-1} . Anal. Calcd for $\text{C}_{28}\text{H}_{25}\text{IrN}_6 \cdot 0.5\text{H}_2\text{O}$: C, 52.00; H, 4.05; N, 12.99. Found: C, 52.35; H, 4.03; N, 12.72. MALDI-TOF-MS m/z 611.65 ($[\text{M}-\text{CN}]^+$, $\text{M} = [\text{C}_{27}\text{H}_{25}\text{IrN}_5\text{CN}]$).

Results and Discussion

Synthesis of Ir(N \wedge C \wedge N)(N \wedge C)X complexes. The tridentate pyrazolyl ligand N \wedge C \wedge N (bpzb, dmbpzb, or dfbpzb) was synthesized according to the method described in the literature^{32–34} except that dibromobenzene was used. The reaction of N \wedge C \wedge N with $\text{IrCl}_3 \cdot n\text{H}_2\text{O}$ in refluxing methanol afforded an insoluble precipitate, which presumably corresponds to chloro-bridged iridium oligomer. Unfortunately, any attempts to characterize the compounds have failed because of its insolubility. Therefore, this insoluble compound was used as it is for further reaction with excess ppy. Further reaction of the insoluble complex with ppy in glycerol by microwave-assisted heating afforded the Ir-(N \wedge C \wedge N)(ppy)Cl complex, where N \wedge C \wedge N = bpzb, dmbpzb, or dfbpzb ligand was used. For the reaction of bpzb with $\text{IrCl}_3 \cdot n\text{H}_2\text{O}$, two coordination modes, namely, the tridentate (mode I) and bidentate fashions (mode II), were possible, as shown in Scheme 1; this yielded a mixture with different coordination modes. Recently, two coordination modes have been already pointed out for the reaction of 1,3-bis(2-pyridyl)benzene with $\text{IrCl}_3 \cdot 3\text{H}_2\text{O}$.³⁵ In the case of bidentate coordination mode of bpzb, one of the probable complexes is $[\text{Ir}_2(\text{bpzb})_4\text{Cl}_2]$, whose structure might be similar to that of $[\text{Ir}_2(\text{ppy})_4\text{Cl}_2]$ (ppy = 2-phenylpyridine). In fact, the ESI-MS spectrum of the reaction product indicated the presence of several complexes, wherein $[\text{Ir}(\text{bpzb})(\text{ppy})\text{Cl}]$, $[\text{Ir}_2(\text{bpzb})_4\text{Cl}_2]$, and $[\text{Ir}_2(\text{ppy})_4\text{Cl}_2]$ are the major compounds. However, we were unable to separate these complexes. To overcome this difficulty, the solubility difference between these complexes after the metathesis

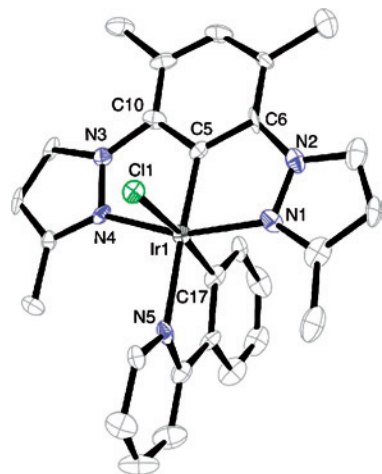
reaction was used. The metathesis reaction of the product mixtures containing $[\text{Ir}(\text{bpzb})(\text{ppy})\text{Cl}]$ and $[\text{Ir}_2(\text{L})_4\text{Cl}_2]$ (L = ppy and bpzb) with KCN yielded neutral $[\text{Ir}(\text{bpzb})(\text{ppy})\text{CN}]$ and anionic $[\text{Ir}(\text{L})_2(\text{CN})_2]^-$ (L = ppy and bpzb), respectively. The latter complex, $[\text{Ir}(\text{L})_2(\text{CN})_2]^-$, was easily extracted into the water phase by using the two-phase CH_2Cl_2 –water system, and thus the desired $[\text{Ir}(\text{bpzb})(\text{ppy})\text{CN}]$ complex remained in CH_2Cl_2 . While the yield is not so good, a pure product of $[\text{Ir}(\text{bpzb})(\text{ppy})\text{CN}]$ was obtained. To prevent the cyclometalation reaction at the C4 or C6 position of the phenyl ring in the tridentate bpzb ligand and also to tune the emission maxima of the complex by electronic effect, a fluoro or methyl group was introduced at the 4,6 positions on the central phenyl ring of bpzb. As a result, two new ligands, 1,3-bis(3-methylpyrazolyl)-4,6-difluorobenzene (dfbpzb) and 1,3-bis(3-methylpyrazolyl)-4,6-dimethylbenzene (dmbpzb), were synthesized accordingly. The introduction of the substituent at the 4,6 positions of the tridentate bpzb ligand can eliminate the possibility of bidentate coordination mode II product, which results in a significant improvement in the product yield.

In the present study, only one isomer was selectively obtained because of strong trans effect of the iridium–carbon bond using a solvent with a high boiling point (glycerol) subjected to microwave irradiation; its structure was determined by using single-crystal X-ray crystallography, as described below.

To investigate the photophysical stability of the complexes, the photoirradiation experiments of $\text{Ir}(\text{dfbpzb})(\text{ppy})\text{Cl}$ in different solvents have been carried out as an example for the present iridium complexes. When the complex was irradiated at a wavelength of 365 nm in CDCl_3 and the reaction was successively monitored by ^1H NMR, many new ^1H signals appeared, indicating that the complex was decomposed under UV irradiation. On the other hand, a clean reaction with isosbestic UV spectral change was observed in CH_3CN , indicating that the chloro substitution reaction in $\text{Ir}(\text{dfbpzb})(\text{ppy})\text{Cl}$ proceeded to yield $[\text{Ir}(\text{dfbpzb})(\text{ppy})(\text{CH}_3\text{CN})]\text{Cl}$. Therefore, a radiationless pathway through the dd state has been considered to be one of the deactivating and reactive channels. The photochemical substitution reaction of the halogeno group in the $[\text{Ir}(\text{L})(\text{ppy})\text{X}]$ complexes (L = Mebib, dfbpzb) is commonly observed.

Crystal Structure of Complex. The perspective view (ORTEP) of the $\text{Ir}(\text{dmbpzb})(\text{ppy})\text{Cl} \cdot \text{CH}_2\text{Cl}_2$ crystal structure is shown in Figure 1. The selected bond distances, angles, and torsion angles are listed in Table 2. The coordination geometry of the Ir(III) centers was distorted octahedral geometry around the iridium atom with one tridentate N \wedge C \wedge N ligand and one ppy ligand as well as a chlorine atom. The Ir–C5 bond in the tridentate N \wedge C \wedge N moiety is located at the trans position of the nitrogen atom in ppy, whereas the Ir–C17 bond in ppy is located at the trans position to chlorine. The cis Ir–C bonding structure is thermodynamically more stable as compared to the trans Ir–C one because the Ir–C bond exhibits a strong trans effect. The Ir–C5 bond length in the N \wedge C \wedge N ligand of the $\text{Ir}(\text{dmbpzb})(\text{ppy})\text{Cl}$ complex is 1.94(1) Å, which is compa-

(35) Wilkinson, A. J.; Goeta, A. E.; Foster, C. E.; Williams, J. A. G. *Inorg. Chem.* **2004**, *43*, 6513.



Ir(dmbpzb)(ppy)Cl

Figure 1. ORTEP diagram of complex Ir(dmbpzb)(ppy)Cl·CH₂Cl₂. Hydrogen atoms and CH₂Cl₂ were omitted for clarity.

Table 2. Selected Bond Lengths and Bond Angles of Ir(III) Complexes

Ir(dmbpzb)(ppy)Cl	
Ir(1)–N(1)	2.048(8)
Ir(1)–N(4)	2.059(7)
Ir(1)–C(5)	1.94(1)
Ir(1)–N(5)	2.13(1)
Ir(1)–C(17)	2.01(1)
Ir(1)–Cl(1)	2.488(2)
N(1)–Ir(1)–Cl(1)	89.3(2)
N(4)–Ir(1)–Cl(1)	90.3(2)
N(5)–Ir(1)–Cl(1)	93.7(2)
C(5)–Ir(1)–Cl(1)	90.7(3)
C(17)–Ir(1)–Cl(1)	172.8(3)
N(4)–Ir(1)–N(1)	158.5(4)
C(5)–Ir(1)–N(1)	79.0(4)
C(17)–Ir(1)–N(1)	91.7(4)
N(5)–Ir(1)–N(4)	100.6(3)
C(5)–Ir(1)–N(4)	79.4(4)
C(17)–Ir(1)–N(4)	91.3(3)
C(5)–Ir(1)–N(5)	175.7(4)
C(17)–Ir(1)–N(5)	79.1(4)
C(17)–Ir(1)–C(5)	96.6(4)

table to the Ir–C (N \wedge C \wedge N) bond length in [Ir(dpyx)-(ttpy)](PF₆)₂ (dpyx = 1,3-di(2-pyridyl)-4,6-dimethylbenzene, ttpy = 4'-tolylterpyridine) (1.954(4) Å)³⁵ and relevant pincer-ligated metal complexes such as [Pt(N \wedge C \wedge N)Cl] (1.89–1.95 Å).^{36,37} The biting bond angles were found between Ir and pyrazolyl nitrogen along with phenyl, that is, C5–Ir1–N4: 79.4(4)° and C5–Ir1–N1: 79.0(4)°, respectively. The relevant bite angle of [Ir(ppz)₃] (ppz = 1-phenylpyrazolyl) has been reported to be 78.7°,^{8a} which is comparable to the present tridentate iridium complex. The Ir–Cl bond length is 2.488(2) Å, which is slightly longer than the bond length of [Ir(Phbib)(ppy)Cl] (2.474 Å) (Phbib = bis(*N*-phenylbenzimidazolyl)benzene).³⁸

Electrochemistry. The electrochemical behaviors of the new Ir(III) complexes were investigated by cyclic voltam-

Table 3. Electrochemical Data for the Ir(III) Complexes^a

complex	$E_{1/2}$ or E_p (ΔE_p)/V (mV)	E_p^{red} /V	ΔE_1 /V
Ir(bpzb)(ppy)CN	0.73 (165)	–2.60 (irr), –2.98 (irr)	3.33
Ir(dfpbz)(ppy)Cl	0.75 (165)	–2.58 (irr), –3.07 (irr)	3.33
Ir(dfpbz)(ppy)CN	0.90 (irr)	–2.52 (irr), –2.95 (irr)	3.42
Ir(dmbpzb)(ppy)Cl	0.52 (172)	–2.66 (irr), –3.12 (irr)	3.18
Ir(dmbpzb)(ppy)CN	0.64 (160)	–2.64 (irr), –3.05 (irr)	3.28

^a Redox measurements were carried out in an anhydrous DMF solution, and all of the values are reported relative to Fc⁰/Fc⁺. At the same condition, the half-wave potential and peak separation of ferrocene were +0.077 V vs Ag⁺/Ag and 150 mV, respectively. ΔE_p = the peak separation value between the anodic and cathodic peaks. Irr = irreversible process. ΔE_1 = $E_{\text{ox}} - E_{\text{red}}$ (first).

metry using glassy carbon as the working electrode, and all of the potentials were referred to the ferrocene/ferrocenium (Fc/Fc⁺) redox potential. The electrochemical data are summarized in Table 3, together with the cyclic voltammograms in the Supporting Information. The Ir(III/IV) oxidation wave appeared from +0.5 to +0.9 V vs Fc/Fc⁺ as a quasi-reversible process except the Ir(dfpbz)(ppy)CN complex, which shows an irreversible one. The Ir(III/IV) oxidation potential is shifted toward the negative direction in the order Ir(dfpbz)(ppy)CN (+0.90 V) > Ir(dfpbz)(ppy)Cl (+0.75 V) > Ir(bpzb)(ppy)CN (+0.73 V) > Ir(dmbpzb)(ppy)CN (+0.64 V) > Ir(dmbpzb)(ppy)Cl (+0.52 V). The oxidation potential of the difluoro-substituted Ir(dfpbz)(ppy)Cl is 0.23 V greater than that of the methyl analogue. Moreover, an oxidation potential greater by 0.1 V is observed for Ir(dmbpzb)(ppy)Cl (+0.52 V) as compared to that for Ir(Mebib)(ppy)Cl (0.42 V) because of the weaker σ -donor property of the pyrazolyl ligands as compared to the benzimidazole one.³⁹ In general, reduction may occur primarily on the low-lying π^* orbitals of the ligand in the relevant iridium complexes. The reduction potentials of the present iridium complexes were almost constant with two irreversible processes centered at around –2.6 and –3.0 V, respectively. A comparison of the reduction potentials of Ir(N \wedge C \wedge N)(ppy)Cl with those of *fac*-Ir(ppz)₃ (–3.2 V) and *fac*-Ir(ppy)₃ (–2.70, –3.00 V) suggests that the first reduction occurs primarily on the ppy ligand, which is supported by the DFT calculations described later. The absence of the reductive process in pyrazolyl complexes is a common occurrence because of higher π^* -orbital energies in the pyrazole derivatives.^{8,40}

Absorption and Emission Properties. The spectroscopic data for the absorption and emission spectra of the complexes are listed in Table 4 and their absorptions (for clarity of the MLCT band, the UV–vis spectra recorded under a high concentration is also included) and emission spectra at 77 K are shown in Figure 2. The absorption spectra of the complexes in dichloromethane show intense bands (ϵ in the range of (1.9~3.8) $\times 10^4$ M^{–1}cm^{–1}) in the UV region around 200–300 nm. These bands are assigned to the $\pi\pi^*$ ligand-centered transition in both the N \wedge C \wedge N and N \wedge C ligands. The bands around 300–350 nm of moderate intensity (ϵ : (6.0~9.0)

(36) Williams, J. A. G.; Beeby, A.; Davies, E. S.; Weinstein, J. A.; Wilson, C. *Inorg. Chem.* **2003**, *42*, 8609.

(37) Jude, H.; Bauer, J. A. K.; Connick, W. B. *Inorg. Chem.* **2002**, *41*, 2275.

(38) Obara, S.; Itabashi, M.; Okuda, F.; Tamaki, S.; Tanabe, Y.; Ishii, Y.; Nozaki, K.; Haga, M. *Inorg. Chem.* **2006**, *45*, 8907.

(39) Luo, Y.; Potvin, P. G.; Tse, Y.-H.; Lever, A. B. P. *Inorg. Chem.* **1996**, *35*, 5445.

(40) Brooks, J.; Babayan, Y.; Lamansky, S.; Djurovich, P. I.; Tsyba, I.; Bau, R.; Thompson, M. E. *Inorg. Chem.* **2002**, *41*, 3055.

Table 4. Photophysical Data for the Ir(N \wedge C \wedge N)(N \wedge C)X Complexes in CH₂Cl₂

complex	$\lambda_{\text{abs}}/\text{nm}$ ($\epsilon: 10^4 \text{ M}^{-1}\text{cm}^{-1}$)	$\lambda_{\text{em}}/\text{nm}^a$		E_{0-0}/eV	Φ (298 K)	$\tau/\mu\text{s}$	
		(77 K)	(77 K)			(298 K)	(77K) ^a
Ir(bpzb)(ppy)CN	256(1.93), 346(0.81), 368sh(0.58)	449, 481, 508,	2.76	5×10^{-3}	0.0047	9.6	
Ir(dfbpzb)(ppy)Cl	258(3.21), 338(0.60), 384(0.23), 411(0.12)	456, 490, 518	2.72	0.4×10^{-3c}	0.00018 ^d	6.0	
Ir(dfbpzb)(ppy)CN	249(2.44), 328(0.64), 368(0.22)	447, 480, 506	2.77	4×10^{-3}	0.0028	13.1	
Ir(dmbpzb)(ppy)Cl	264(3.63), 320(0.86), 348(0.82), 369(0.55), 419(0.16)	460, 493, 522	2.70	0.5×10^{-3c}	0.00079 ^d	3.9	
Ir(dmbpzb)(ppy)CN	254(3.82), 341(0.67), 356sh(0.56)	449, 481, 508	2.76	8×10^{-3}	0.014	8.1	
<i>fac</i> -Ir(ppy) ₃ ^b	244(4.55), 283(4.48), 341(0.92), 377(1.20), 405(0.81), 455(0.28), 488(0.16)	492	2.52	0.40	1.9	3.6	
<i>fac</i> -Ir(ppz) ₃ ^b	244(4.91), 261(1.41), 292(1.65), 321(1.35), 366(0.42)	414	3.00			14.0	

^a In CH₂Cl₂:toluene (1:1 v/v). ^b Ref 8. ^c Estimated by extrapolating the linear relationship of Φ versus T^{-1} in the range of 193–223 K. ^d Estimated by extrapolating the Arrhenius plots in the range of 193–253 K.

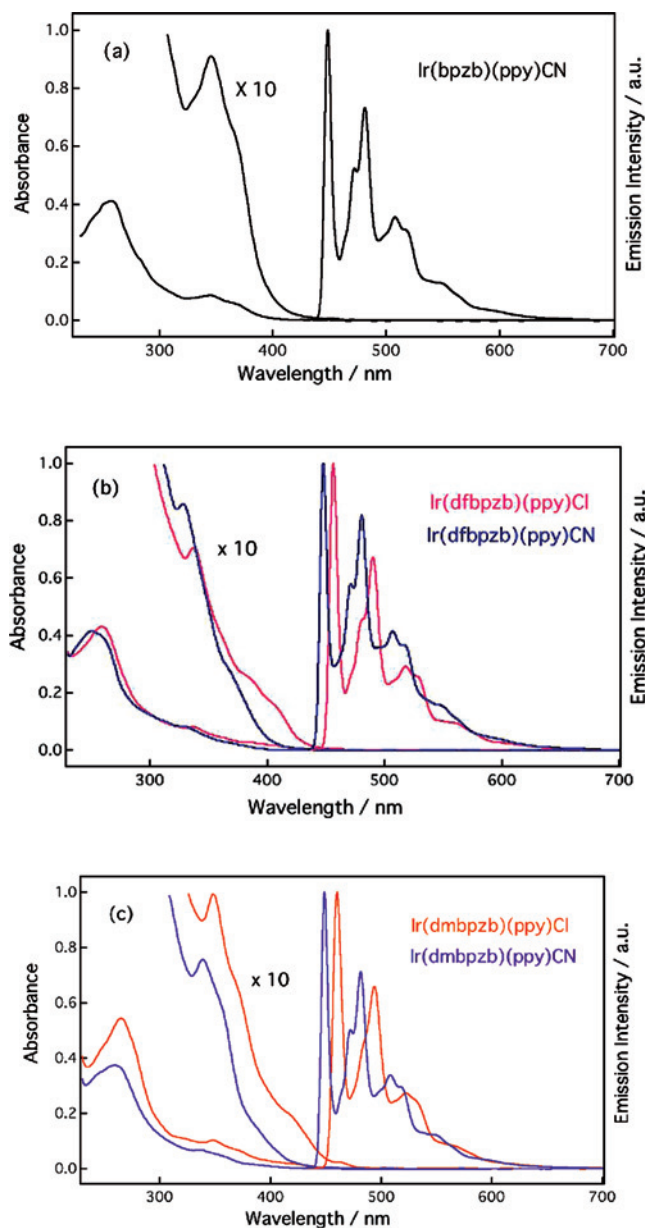


Figure 2. UV-vis (CH₂Cl₂, room temperature) and emission spectra (CH₂Cl₂/toluene, 1:1 v/v, 77 K) of the Ir(III) complexes: (a) Ir(bpzb)(ppy)CN, (b) Ir(dfbpzb)(ppy)X (X = Cl and CN), and (c) Ir(dmbpzb)(ppy)X (X = Cl and CN).

$\times 10^3 \text{ M}^{-1}\text{cm}^{-1}$) are also assigned to the $\pi\pi^*$ transition of the N \wedge C \wedge N ligand. Several weak absorption bands were observed in the longer wavelength region as a shoulder, which can be assigned to the metal-to-ligand charge transfer (¹MLCT) transi-

tions involving either the N \wedge C \wedge N or the N \wedge C ligand. Upon the substitution of Cl by CN, a shorter wavelength shift of both $\pi\pi^*$ and MLCT bands was observed. The introduction of electron-withdrawing difluoro groups in the N \wedge C \wedge N ring also results in a higher energy shift of the MLCT band as compared to that of the methyl or hydrogen group. Moreover, much weaker absorption bands at still lower energies ($\lambda > 410 \text{ nm}$) observed in the concentrated solutions of the complexes can be attributed to the ³LC (ligand-centered) transitions mixed with ³MLCT, as supported by the emission feature.⁷

The emission intensities of all of the complexes are very weak or even nonemissive in degassed CH₂Cl₂ at room temperature, whereas the complexes exhibit unique blue emission at low temperatures. As shown in Figure 2, the emission spectra observed for the complexes at 77 K are highly structured, exhibiting a considerable LC characteristic. It should be mentioned that the spectral profiles of the Ir(III) complexes herein resemble those of Rh(ppy)₃.⁴¹ In combination with the fact that varying the substituents on N \wedge C \wedge N does not significantly affect the spectral features indicates that N \wedge C \wedge N plays a less important role in the lowest excited state than that of ppy. It can be inferred that the excited electron resides mainly on the ppy ligand, which is in accordance with the above electrochemical results.

The 0–0 transition energies to the phosphorescence states were estimated as the highest energy peak in the emission spectra at 77 K. The order of the 0–0 energies, Ir(dfbpzb)(ppy)CN > Ir(bpzb)(ppy)CN \cong Ir(dmbpzb)(ppy)CN > Ir(dfbpzb)(ppy)Cl > Ir(dmbpzb)(ppy)Cl, is in accordance with the ΔE_1 value ($E_{\text{ox}} - E_{\text{red}}$ (1st)), except that the order of Ir(dfbpzb)(ppy)Cl and Ir(dmbpzb)(ppy)CN was reversed. The substitution of phenyl hydrogen atoms with inductive electron-withdrawing fluorine atoms stabilized the HOMO energies more than the LUMO ones, thereby increasing the triplet energy gap. In comparison with the emission energy of *fac*-Ir(ppz)₃ ($E_{0-0} = 414 \text{ nm}$, 3.00 eV) and *fac*-Ir(ppy)₃ ($E_{0-0} = 494 \text{ nm}$, 2.51 eV), the emission energy of the mixed-ligand complexes (2.70–2.76 eV) lies at the midpoint between those of the *fac*-Ir(ppz)₃ and *fac*-Ir(ppy)₃. The substitution from benzimidazolyl groups [Ir(L1)(bpy)Cl]-(PF₆)₂ (L1 = 2,6-bis(methyl-benzimidazol)-2-yl)pyridine, bpy = 2,2'-bipyridine) to the pyrazolyl ones in Ir(N \wedge C \wedge N)(N \wedge C)Cl induces a blue shift of more than 50 nm in the emission maxima.²⁴ At the same time, the substitution from 1,3-di(2-

(41) Colombo, M. G.; Brunold, T. C.; Riedener, T.; Guedel, H. U.; Fortsch, M.; Büergi, H.-B. *Inorg. Chem.* **1994**, *33*, 545.

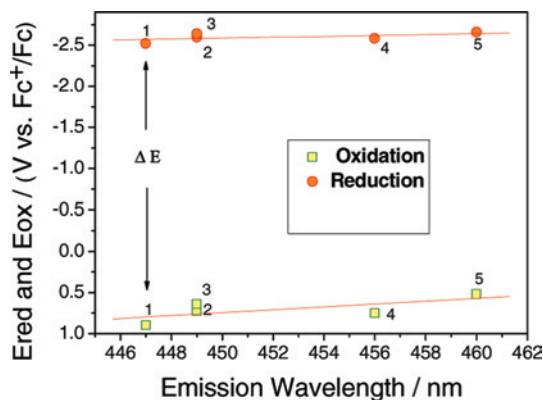


Figure 3. Plots of the 0–0 transition emission wavelength vs redox potential for the iridium complexes: 1, Ir(dfbpzb)(ppy)CN; 2, Ir(bpzb)(ppy)CN; 3, Ir(dmbpzb)(ppy)CN; 4, Ir(dfbpzb)(ppy)Cl; and 5, Ir(dmbpzb)(ppy)Cl.

pyridyl)-4,6-dimethylbenzene (dpyx) to the tridentate pyrazolyl ligand also induces a blue shift of approximately 30 nm in the emission maxima.²⁵ These facts are reflected in the higher energy of the π^* -orbital level in the pyrazolyl ligand as compared to those for the benzimidazolyl and pyridyl ligands, resulting in the larger HOMO–LUMO energy gap.

As shown in Table 4, the photoluminescence quantum yields of the iridium complexes with the pyrazolyl ligands are much lower than 10^{-2} and the lifetimes are very short (0.2–14 ns) at ambient temperature. The lifetimes decrease in the order of dmbpzb > bpzb > dfbpzb. It is worthy to note that the complexes with chloride ($X=Cl$) are much short-lived compared to those for $X=CN$. The radiative rates (k_r) for these complexes are in the range of $0.6 \times 10^5 \text{ s}^{-1}$ to $2 \times 10^6 \text{ s}^{-1}$, comparable to those of the highly emissive Ir(Mebib)(ppy)X ($k_r \sim 10^6 \text{ s}^{-1}$).³⁸ Whereas the present complexes are short-lived at ambient temperature, the lifetimes at 77 K were found to be within 3–14 μs . The long emission lifetime, in combination with the vibronic spectral features, lead us to assign the emission to be originating from the triplet manifold in which the ^3LC configuration may have a dominant contribution to this transition than that of $^3\text{MLCT}$. The lifetimes of our complexes are longer than those of the iridium–pyrazolyl–triazolyl mixed-ligand complexes, as reported by Yang et al.⁷

For the present new Ir(III) complexes, the plots of the 0–0 transition energy versus the redox potential are shown in Figure 3. Upon increasing the Ir(III/IV) oxidation potentials, the emission maximum is shifted to a shorter wavelength. On the other hand, the reduction potentials keep almost constant. Therefore, the introduction of the electron-withdrawing groups into the phenyl ring or the substitution of chlorine to CN leads to the lowering of the HOMO energy, resulting in the blue emissions. The same effect has been reported for *fac*-Ir($F_2\text{ppy}$)₃.^{8,10}

Temperature-Dependent Lifetime Measurement. The emission decay of Ir(dfbpzb)(ppy)Cl in an argon-saturated toluene/1-chloropropane (1:1) mixed solvent was measured in the temperature range of 90–300 K, and the decay rate constants were determined from the time profile of the

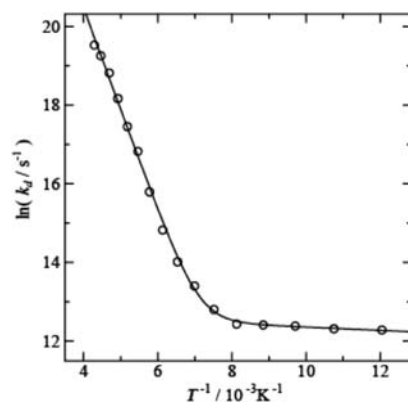


Figure 4. Temperature variation in the emission decay rate constants of Ir(dfbpzb)(ppy)Cl in an argon-saturated toluene/1-chloropropane (1:1) mixed solvent. The solid line indicates the curve calculated using eq 1 with the parameters of $A_1 = 2.3 \times 10^{13} \text{ s}^{-1}$, $E_{a1} = 1720 \text{ cm}^{-1}$, $A_2 = 3.5 \times 10^5 \text{ s}^{-1}$, and $E_{a2} = 27 \text{ cm}^{-1}$.

Table 5. Selected Bond Lengths and Dihedral Angle of the Structures Calculated for Ground State (GS), Phosphorescent State (P), Lowest dd State, and Transition States for $P \rightarrow dd$ and for $dd \rightarrow GS$ in Ir(dfbpzb)(ppy)Cl and Ir(Mebib)(ppy)Cl

	GS (obsd)	P	TS1 (P \rightarrow dd)	dd	TS2 (dd \rightarrow GS)
Ir(dfbpzb)(ppy)Cl					
Ir(1)–N(1)	2.05	2.05	2.20	2.44	2.65
Ir(1)–N(5)	2.12	2.11	2.11	2.10	2.10
Ir(1)–C(5)	1.94	1.95	1.99	2.03	2.00
Ir(1)–C(17)	2.01	2.02	2.02	2.03	2.01
Ir(1)–Cl(1)	2.52	2.50	2.51	2.47	2.45
N(4)–N(3)–C(6)–C(5)	0.3	0.4	10.3	8.6	18.8
Ir(Mebib)(ppy)Cl					
Ir(1)–N(1)	2.04(2.07) ^a	2.01	2.25	2.44	2.65
Ir(1)–N(5)	2.12(2.16) ^a	2.11	2.11	2.10	2.10
Ir(1)–C(5)	1.95(1.92) ^a	1.97	1.99	2.02	2.02
Ir(1)–C(17)	2.01(2.00) ^a	2.14	1.99	2.02	2.02
Ir(1)–Cl(1)	2.52(2.49) ^a	2.48	2.46	2.48	2.46
N(4)–C(7)–C(6)–C(5)	0.9	1.7	5.4	14.0	29.1

^a Ref 38.

emission intensity at 470 nm. The temperature dependence of the rate constants exhibited a biphasic behavior, as shown in Figure 4: the rate constants were almost unchanged in the range from 90 to 120 K, whereas they increased steeply above 120 K. The biphasic behavior of the decay rates were analyzed according to the so-called three-state model involving the ground state, an emitting state, and a higher-lying nonemitting short-lived state.^{42–44} In this model, the temperature-dependent decay rates are given by the sum of two Arrhenius equations:

$$k_d(T) = A_1 \exp(-E_{a1}/kT) + A_2 \exp(-E_{a2}/kT) \quad (1)$$

where A_1 and E_{a1} are the frequency factor and activation energy for the thermal deactivation through the higher-lying excited state, respectively, and A_2 and E_{a2} are those for the deactivation directly from the emitting state to the ground state. Fitting the data shown in Figure 4 to eq 1 yields the

(42) Durham, B.; Casper, J. V.; Nagle, J. K.; Meyer, T. J. *J. Am. Chem. Soc.* **1982**, *104*, 4803.

(43) Allen, G. H.; White, R. P.; Rillema, D. P.; Meyer, T. J. *J. Am. Chem. Soc.* **1984**, *106*, 2613.

(44) (a) Sykora, M.; Kincaid, J. R. *Inorg. Chem.* **1995**, *34*, 5852. (b) Benniston, A. C.; Chapman, G.; Harriman, A.; Mehrabi, M.; Sams, C. A. *Inorg. Chem.* **2004**, *43*, 4227.

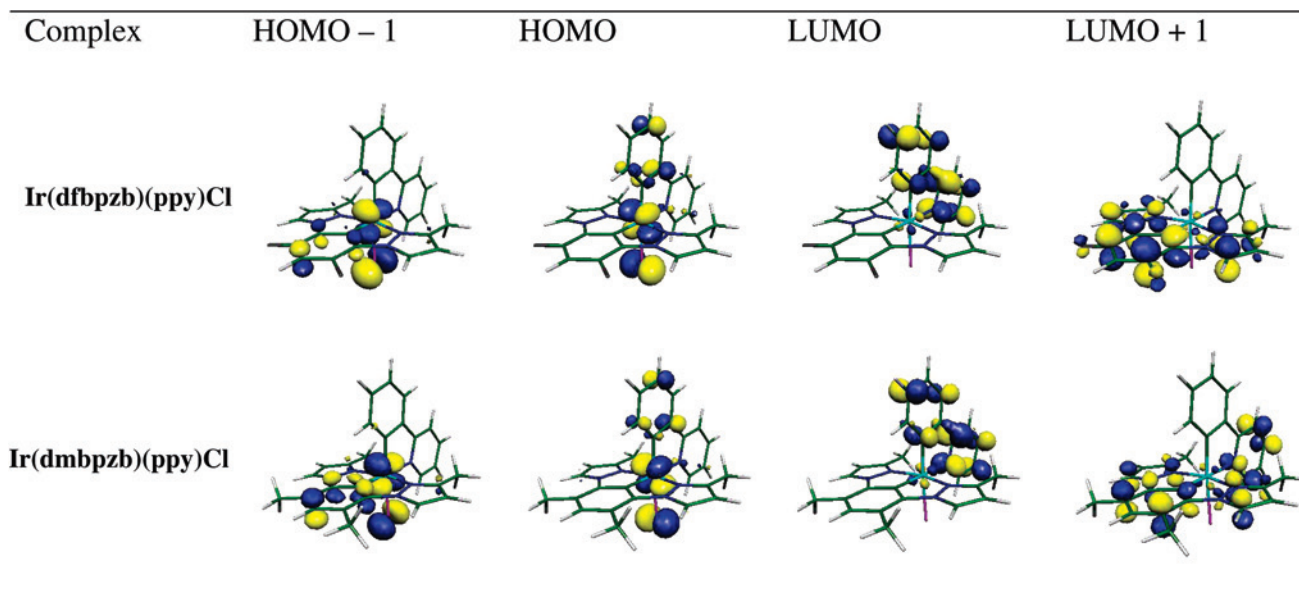


Figure 5. Frontier molecular orbitals of the complex Ir(dfbpzb)(ppy)Cl and Ir(dmbpzb)(ppy)Cl calculated at the PBE1PBE/BSI level for the geometries optimized for T₁.

kinetic parameters ($A_1 = 2.3 \times 10^{13} \text{ s}^{-1}$, $E_{a1} = 1720 \text{ cm}^{-1}$) for the thermal deactivation process. Interestingly, these parameters are similar in magnitude to those for $[\text{Ru}(\text{terpy})_2]^{2+}$, (terpy = 2,2':6'2''-terpyridine) ($2 \times 10^{13} \text{ s}^{-1}$ and 1680 cm^{-1}) of which the MLCT state is well-known to be quenched by the closely lying ^3dd excited state.⁴⁵ As in the case for $[\text{Ru}(\text{terpy})_2]^{2+}$, such a high frequency factor indicates that the rate-determining step of the thermal deactivation process should be at the potential energy crossing either $^3\text{MLCT} \rightarrow ^3\text{dd}$ or $^3\text{dd} \rightarrow ^1\text{GS}$.⁴⁶ In the former, the observed E_{a1} value corresponds with the energy gap between the $^3\text{MLCT}$ and $^3\text{MLCT} \rightarrow ^3\text{dd}$ intersection, whereas in the latter, it corresponds to the energy difference between the $^3\text{MLCT}$ and $^3\text{MLCT} \rightarrow ^1\text{GS}$ intersection. A low E_{a2} value of 27 cm^{-1} is related to the zero-field splitting of the lowest triplet state due to the second-order spin-orbit coupling of the 5d electron.⁴⁷ A small frequency factor of $A_2 = 3.5 \times 10^5 \text{ s}^{-1}$ is consistent with the nonadiabatic transition involving the unfavorable overlapping of the vibrational wave functions between the emitting state and the vibrationally excited ground states.

DFT Calculations. To better understand the photophysical properties of the complexes, the electronic structures of Ir(dfbpzb)(ppy)Cl and Ir(dmbpzb)(ppy)Cl were calculated. The geometries of the ground state (GS) were optimized at the PBE1PBE/BSI level, and then the excited states emitting the phosphorescence were optimized at the unrestricted PBE1PBE/BSI level as the lowest state with the triplet multiplicity using the GS geometries as the initial structure. The selected geometrical parameters for Ir(dfbpzb)(ppy)Cl are listed in Table 5 together with those for Ir(Mebib)(ppy)Cl. Most of the bond lengths for the GS of Ir(Mebib)-

(ppy)Cl are in excellent agreement with those of the crystallographic one.

The features of the frontier orbitals in the phosphorescent geometries are shown in Figure 5. Apparently, the HOMOs for both these complexes are mainly based on the iridium, chlorine, and phenyl moieties in the ppy ligands. As shown in Figure 5, d orbitals are also involved in the HOMOs, whereas the LUMOs are mostly distributed over the ppy moiety. Time-dependent DFT (TDDFT) calculations indicated that the T₁ state mainly involves the HOMO \rightarrow LUMO transition, and thus the phosphorescent state is an admixture of the MLCT (Ir \rightarrow ppy), XLCT (Cl \rightarrow ppy), and $\pi\pi^*$ (ppy) states.

DFT Study of Deactivation Pathway. The photophysical properties of the Ir(L)(ppy)Cl complexes (L = dmbpzb and dfbpzb) are in considerable contrast with those of the highly emissive Ir(Mebib)(ppy)Cl complex.³⁸ Both these complexes exhibit strong emissions with microsecond lifetimes at 77 K. The lifetime of the dfbpzb complex, however, is fairly short (less than 1 ns) at the ambient temperature, whereas the lifetime of the Mebib complex is almost unchanged over a wide range of temperatures (77–300 K). Extensive studies of Ru(II) polypyridyl complexes reveal that such thermal quenching of the emissive state of the d⁶ metal complexes can be ascribed to the deactivation via thermally accessible dd states.^{42–44} To obtain insights into the deactivation process of the phosphorescent state, the potential energy curves for this deactivation via the lowest dd state in the Ir(dfbpzb)(ppy)Cl and Ir(Mebib)(ppy)Cl complexes were calculated at the unrestricted DFT level according to the following procedure.

(45) Juris, U. A.; Balzani, V.; Barigelli, F.; Campagna, S.; Belser, P.; von Zelewsky, A. *Coord. Chem. Rev.* **1988**, *84*, 85.

(46) Islam, A.; Ikeda, N.; Nozaki, K.; Ohno, T. *Chem. Phys. Lett.* **1996**, *263*, 209.

(47) Nozaki, K. *J. Chin. Chem. Soc.* **2006**, *53*, 101.

(6) (a) Kwon, T.-H.; Cho, H. S.; Kim, M. K.; Kim, J.-W.; Kim, J.-J.; Lee, K. H.; Park, S. J.; Shin, I.-S.; Kim, H.; Shin, D. M.; Chung, Y. K.; Hong, J.-I. *Organometallics* **2005**, *24*, 1578. (b) Yu, J. -K.; Hu, Y.-H.; Cheng, Y.-M.; Chou, P.-T.; Peng, S.-M.; Lee, G. -H.; Carty, A. J.; Tung, Y. -L.; Lee, S. -W.; Chi, Y.; Liu, C. -S. *Chem.-Eur. J.* **2004**, *10*, 6255. (c) Karatsu, T.; Ito, E.; Yagai, S.; Kitamura, A. *Chem. Phys. Lett.* **2006**, *424*, 353.

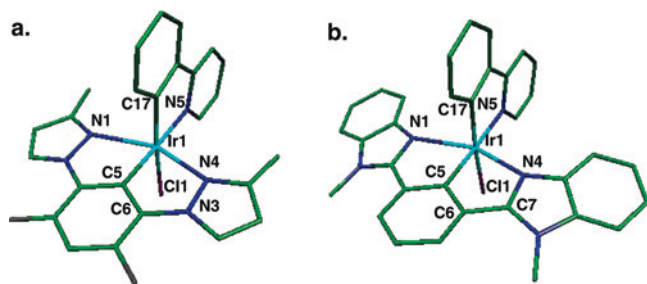


Figure 6. Geometries of the lowest dd states calculated at the UPBE1PBE/BSL level for [Ir(dfbpzb)(ppy)Cl] (a) and [Ir(Mebib)(ppy)Cl] (b).

Step 1. To determine the geometry of the lowest triplet dd states that are evidently involved in the deactivation process, preliminary geometrical optimizations were performed with constraints that one of the six metal-to-ligand bond lengths was elongated by 20–30% of the GS geometry. The geometry with the least SCF energy among the six preliminary geometries was then optimized without these geometrical constraints. In the resulting geometry for Ir(dfbpzb)(ppy)Cl, the highest singly occupied orbitals are mainly $d\sigma^*$ of Ir(1)–N(1) and Ir(1)–N(4) bonds and the second highest singly occupied orbitals are mainly $d\pi$ of iridium 5d, which is the characteristic of the dd electronic configuration.

Step 2. To find the deactivation pathway of the phosphorescent states, the potential energy surfaces (PESs) of the T_1 state were computed as a function of two geometrical parameters that change the most between the GS and the lowest dd structures. The bond lengths of Ir(1)–N(1) and Ir(1)–N(4) were selected as parameters for the PESs for both the complexes. T_1 -PESs were calculated by using the constrained geometry optimization method at the UPBE1PBE/BSI level when the variations in the bond lengths were in the range of 1.95–2.85 Å for every 0.1 Å. Then, for all the optimized geometries, the SCF energies of the T_1 and S_0 states were calculated at the UPBE1PBE/BSII level, and the resultant mesh data were interpolated using a 2D Spline⁴⁸ to sketch smooth PESs. From the PESs, the deactivation pathway from the phosphorescent state to the ground state was determined as the route having the lowest thermal barrier.

Step 3. The deactivation pathway with the lowest activation energy was found from the PESs. The potential energy curves along the deactivation pathway were calculated in detail to determine the thermal barriers of the transition states.

The calculated geometries for the lowest dd states are shown in Table 5 and Figure 6. The bond lengths of Ir(1)–N(1) and Ir(1)–N(4) in Ir(dfbpzb)(ppy)Cl increase considerably (2.44 Å), whereas the other bond lengths are almost the same as those in the ground state. In addition, the twisting of the pyrazolyl groups in the dfbpzb ligand induces an out-of-plane deformation. Further, for the dd state of Ir(Mebib)(ppy)Cl, the bond lengths of Ir(1)–N(1) and

Ir(1)–N(4) increase considerably (2.44 Å) and the benzimidazolyl groups become twisted.

Parts a and b of Figure 7 show the PESs for Ir(dfbpzb)(ppy)Cl and Ir(Mebib)(ppy)Cl, respectively, which are illustrative for understanding the thermal deactivation of the phosphorescent states in transition metal complexes. The vertical axis of the plots indicates the SCF energy relative to that for S_0 at the geometry optimized for the GS. For both the Ir(III) complexes, the T_1 -PESs have their minima corresponding to the phosphorescent states (denoted by P in Figure 7) around the geometry similar to that for the GS. Therefore, when the complex is excited, the resultant Franck–Condon states are relaxed into the potential minima P. Broad minima in which both the Ir–N bond lengths are 2.4 Å correspond to the dd states. Due to the energy barrier existing between the P and dd (TS_1) states, the excited states are trapped in the potential minima P at low temperatures and decay without passing through the dd states. At high temperatures, when the excited states have sufficient thermal energy to go beyond the humps at TS_1 , they can reach the potential minima dd. It should be noted that the T_1 -PESs around the dd states are considerably shallow, allowing a large distortion of the molecular structure with small thermal activation. With elongation of the Ir–N bond lengths by 0.4 Å from the dd geometry, the excited states can reach the intersections between T_1 -PES and S_0 -PES (TS_2) where very fast deactivation of excited state could take place. Thus, the PES calculations reveal that the thermal deactivation pathway of the phosphorescent state for these Ir(III) complexes is $P \rightarrow TS_1 \rightarrow dd \rightarrow TS_2 \rightarrow GS$. At TS_1 , the electron in the π^* orbital of the ligands needs to be transferred to $d\sigma^*$ of Ir(III). Although the π^* and $d\sigma^*$ orbitals are orthogonal in octahedral structures, they are considerably mixed at TS_1 due to twisting of the pyrazolyl groups in the dfbpzb ligand (dihedral angle N(4)–N(3)–C(6)–C(5) is 10.3°).

The details of the potential-energy curves for the thermal deactivation pathway are shown in Figure 8. Because the energies for S_0 are calculated at the geometries optimized for T_1 , the S_0 energies at 2.05 Å – where the T_1 -PESs have their minima – are equal to the reorganization energy for phosphorescence, approximately 0.25 eV, for both the complexes. Assuming that the difference in the zero-point energy between S_0 and T_1 is negligible, the energy at the bottom of the well P corresponds to the 0–0 transition energy. The energies are 2.66 eV for Ir(dfbpzb)(ppy)Cl and 2.21 eV for Ir(Mebib)(ppy)Cl, which are in excellent agreement with the observed 0–0 transition energies (2.70 and 2.32 eV, respectively) determined from the highest energy peak in the emission spectra at 77 K. The energy of the phosphorescent state for Ir(dfbpzb)(ppy)Cl is 0.45 eV higher than that for Ir(Mebib)(ppy)Cl because the low σ - and π -donor character of the dfbpzb ligand increases the energy level of the MLCT electronic configuration. However, the low σ -donor character decreases the ligand-field splitting, and thereby the energy of the dd state involving $d\sigma^*$ of the Ir–N (pyrazolyl) bonds is 0.25 eV lower than that of the dd state involving $d\sigma^*$ of the Ir–N (benzimidazolyl) bonds in

(48) Press, W. H.; Flannery, B. P.; Teukolsky, S. A.; Vetterling, W. T. *Numerical Recipes in C, Second Edition*; Cambridge University Press: New York, 1992; 10011–4211.

(49) (a) Barigelletti, F.; Juris, A.; Balzani, V.; Belser, P.; Zewlewsky, A. J. *Phys. Chem.* **1987**, *91*, 1095. (b) Frink, M. E.; Sprouse, S. D.; Goodwin, H. A.; Watts, R. J.; Ford, P. C. *Inorg. Chem.* **1988**, *27*, 1283.

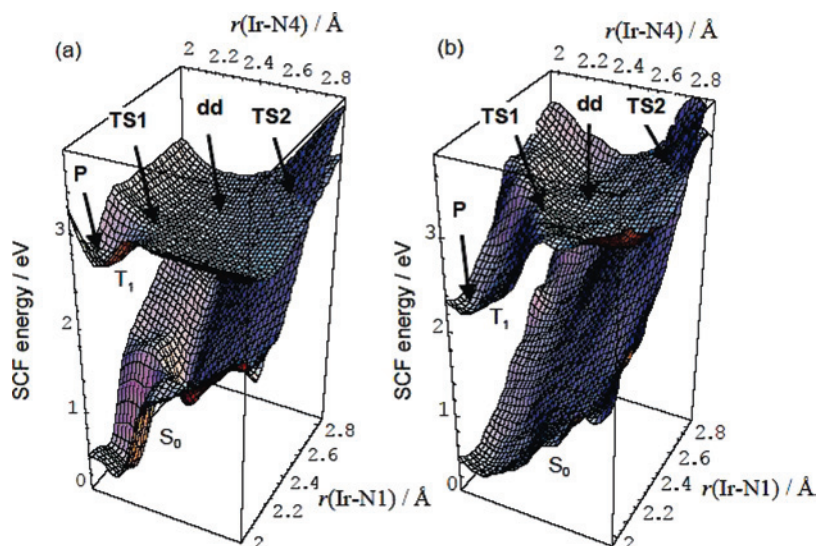


Figure 7. Potential energy surfaces of T1 and S0 calculated as a function of the bond lengths of Ir(1)–N(1) and Ir(1)–N(4) for [Ir(dfbpzb)(ppy)Cl] (a) and for [Ir(Mebib)(ppy)Cl] (b).

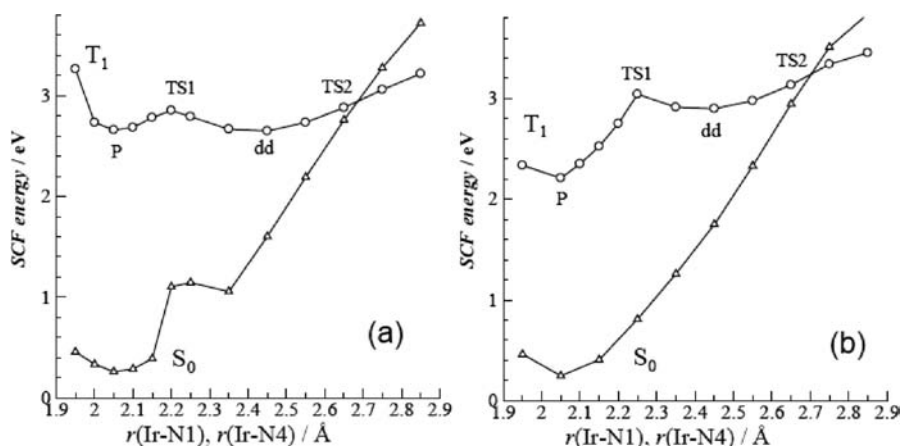


Figure 8. Potential-energy curves involving the thermal deactivation of the phosphorescent state (P) calculated as a function of the bond length Ir(1)–N(1) (Ir(1)–N(4)) for [Ir(dfbpzb)(ppy)Cl] (a) and for [Ir(Mebib)(ppy)Cl] (b).

Ir(Mebib)(ppy)Cl. As a result, the energy minimum of the dd state is almost the same as that for the phosphorescent state P for Ir(dfbpzb)(ppy)Cl (part a of Figure 8), whereas the dd state of Ir(Mebib)(ppy)Cl lies at 0.7 eV above the P state (part b of Figure 8).

For Ir(dfbpzb)(ppy)Cl, the saddle point between the P and dd states lies at 0.20 eV (1600 cm^{-1}) relative to that of P, whereas the transition state between dd and GS is at 0.22 eV (1800 cm^{-1}). It is noteworthy that these calculated values are very close to the observed activation energy (1720 cm^{-1}) for the emission decay process. For Ir(Mebib)(ppy)Cl, deactivation via the dd state is strongly endothermic and could not accelerate the decay rate even at room temperature. Assuming that the frequency factor is the same for Ir(dfbpzb)(ppy)Cl, the deactivation rate via the dd state is calculated to be 1.3 s^{-1} at 300 K, which is five times lower than the rate of the direct decay to GS ($5 \times 10^5\text{ s}^{-1}$).

The following two limiting cases have been proposed for the thermal deactivation of P through dd in Ru(II) polypyridine complexes.⁴⁴

Case I: The rate-determining step (rds) is at the internal conversion from P to dd, and dd deactivates rapidly once it

is produced. The observed activation energy corresponds to the energy difference between the bottom of P and the transition state of the internal conversion.

Case II: P and dd are in equilibrium and the rds is either a nonadiabatic transition from the bottom of the well of dd or a transition at the intersection with S_0 –PES.

The observed high-frequency factor ($A = 2.3 \times 10^{13}\text{ s}^{-1}$) strongly suggests that the rds is at the intersection between the potential energy curves and not the nonadiabatic transition induced by quantum mechanical tunneling effects.⁴⁶ This idea is supported by the fact that the decay rate of the dd states of the Rh(III) polypyridine compounds is approximately 10^5 s^{-1} at 77 K in the glass matrix.⁴⁷ Therefore, the rds of the thermal deactivation for Ir(dfbpzb)(ppy)Cl would be the intersection at either TS1 or TS2. The DFT calculations, however, predict that the energy levels of TS1 and TS2 are almost the same (part a of Figure 8); therefore, it is difficult to determine the rds for the deactivation process. In either case, the lowest excited state of this complex must be short lived at ambient temperature due to the existence of thermally accessible intersection between T_1 –PES and S_0 –PES.

Conclusions

Novel mixed-ligand Ir(III) complexes having the general formula $[\text{Ir}(\text{L})(\text{ppy})\text{X}]$, where L(tridentate) = bis(pyrazolyl)-benzene and ppy(bidentate) = phenylpyridine derivatives, were synthesized. These complexes exhibited unique blue emissions with the 0–0 transitions centered at 447–460 nm at 77 K and with moderately long lifetimes (3–14 μs) at low temperatures. The lack of emissions at the ambient temperature is mainly due to a deactivation process with relatively low activation energy of 1720 cm^{-1} . The DFT calculation revealed the geometry and energy level of the higher-lying dd states involved in the deactivation process. In this study, we demonstrated that the excited-state PESs calculated at the UDFT level provide crucial information not only on the thermal deactivation pathways but also on the thermal barrier. Furthermore, we proposed an effective method to formulate a map to find the deactivation pathway via the dd state in such a large transition-metal complex.

The next step in the future study will be to design the ligands and complexes that will increase the energy separation between the emissive and nonemissive states, leading to higher luminance efficiencies.

Acknowledgment. M.H. gratefully acknowledges the financial support from the Institute of Science and Engineering at Chuo University, the Ministry of Education, Science, Sports and Culture (Monkasho) for a Grant-in-Aid for Scientific Research (No. 19550071). K.N. gratefully acknowledges Monkasho for a Grant-in-Aid for Scientific Research (No. 18550054).

Supporting Information Available: CIF file of Ir(dmbpz)-(ppy)Cl·CH₂Cl₂, cyclic and differential pulse voltammograms of Ir(dfbpz)(ppy)CN, Ir(dfbpz)(ppy)Cl, Ir(bpz)(ppy)CN, Ir(dmbpz)(ppy)CN, and Ir(dmbpz)(ppy)Cl in DMF (0.1 M TBABF₄). This material is available free of charge via the Internet at <http://pubs.acs.org>.

IC800196S